SIMULTANEOUS LINEARIZED INVERSION OF VELOCITY AND DENSITY PROFILES FOR MULTIDIMENSIONAL ACOUSTIC MEDIA

by

Ali Ozbek
Department of Electrical Engineering and Computer Science
and
Earth Resources Laboratory
Massachusetts Institute of Technology
Cambridge, MA 02139

Bernard C. Levy
Department of Electrical Engineering and Computer Science
University of California
Davis, CA 95616

Report Documentation Page

1. REPORT DATE **MAY 1989**	2. REPORT TYPE	3. DATES COVERED **00-05-1989 to 00-05-1989**

4. TITLE AND SUBTITLE	5a. CONTRACT NUMBER
Simultaneous Linearized Inversion of Velocity and Density Profiles for Multidimensional Acoustic Media	5b. GRANT NUMBER
	5c. PROGRAM ELEMENT NUMBER
6. AUTHOR(S)	5d. PROJECT NUMBER
	5e. TASK NUMBER
	5f. WORK UNIT NUMBER

7. PERFORMING ORGANIZATION NAME(S) AND ADDRESS(ES) **Massachusetts Institute of Technology,Laboratory for Information and Decision Systems,77 Massachusetts Avenue,Cambridge,MA,02139-4307**	8. PERFORMING ORGANIZATION REPORT NUMBER
9. SPONSORING/MONITORING AGENCY NAME(S) AND ADDRESS(ES)	10. SPONSOR/MONITOR'S ACRONYM(S)
	11. SPONSOR/MONITOR'S REPORT NUMBER(S)

12. DISTRIBUTION/AVAILABILITY STATEMENT
Approved for public release; distribution unlimited

13. SUPPLEMENTARY NOTES

14. ABSTRACT

15. SUBJECT TERMS

16. SECURITY CLASSIFICATION OF:			17. LIMITATION OF ABSTRACT	18. NUMBER OF PAGES	19a. NAME OF RESPONSIBLE PERSON
a. REPORT **unclassified**	b. ABSTRACT **unclassified**	c. THIS PAGE **unclassified**		**42**	

ABSTRACT

The multidimensional inverse scattering problem for an acoustic medium is considered within the homogeneous background Born approximation. The medium is probed by wide-band plane wave sources, and the scattered field is observed along straight-line receiver arrays. The objective is to reconstruct simultaneously the velocity and density profiles of the medium. The time traces observed at the receivers are appropriately filtered to obtain generalized projections of the velocity and density scattering potentials, which are related to the velocity and density perturbations of the medium with respect to their nominal values. The generalized projections are weighted integrals of the scattering potentials; in two dimensions the weighting functions are concentrated along parabolas, in three dimensions they are concentrated over circular paraboloids. The reconstruction problem for the generalized projections is formulated in a way similar to the problem of x-ray, or straight-line tomography. The solution is expressed as a backprojection operation followed by a two or three dimensional space-invariant filtering operation. In the Fourier domain, the resulting image is a linear combination of the velocity and density scattering potentials, where the coefficients depend on the angle of incidence of the probing wave. Therefore, two or more different angles of incidence are necessary to reconstruct the velocity and density scattering potentials separately.

INTRODUCTION

In this paper, we consider the multidimensional inverse scattering problem for an acoustic medium within the homogeneous background Born approximation. An acoustic medium is probed by wide-band plane wave sources, and the scattered field is observed along straight-line receiver arrays. The objective is to reconstruct simultaneously the velocity and density profiles of the medium.

The 1-D velocity/density profile inversion problem has been studied by a number of researchers, including Raz (1981a), Coen (1981), Hooshyar and Razavy (1983), Yagle and Levy (1984). This problem can in principle be solved exactly.

The multidimensional problem, where the velocity and density profiles are allowed to vary in two or three dimensions, has also interested several researchers. For the multidimensional problem, no exact solution exists. Several approximate inversion techniques have been proposed, which linearize the scattering integral equations by using the Born or Rytov approximations. In this context, it was shown that the experimental requirements of single parameter inversion problems, where the medium density is constant and only the velocity varies, and of multiparameter inversion problems, where both the density and the velocity need to be reconstructed, are different. For the single parameter case, a single scattering experiment is sufficient to – at least partially – reconstruct the object of interest, whereas several experiments are necessary for multiparameter problems.

Raz (1981b), and Clayton and Stolt (1981) have solved the multidimensional problem for an experimental setup where sources and receivers are available at all points on a plane, and scattered waves are measured at all frequencies. Coen, Cheney and Weglein (1984), and Ramm and Weglein (1984) have solved the same

problem for a complete set of sources and receivers, but using only two temporal frequencies. Hooshyar and Weglein (1986) have used two wide-band point sources, where the distance between the sources is required to be small compared to the distance from the sources to the scatterers. Beylkin and Burridge (1987) have presented a solution for a medium with a variable background, with sources and receivers surrounding the medium.

The class of problems where the medium is probed by plane waves has been investigated by Norton and Devaney. Norton (1983) has used a flat transducer as a source of wide-band, plane wave illumination, and as a receiver of the backscattered waves. A second transducer, oriented at a different angle with respect to the first, is used as a receiver only. The two transducers are rotated together 180° around the object, and the scattered waves are recorded at all angles during the rotation. Devaney (1985) has extended the diffraction tomography theory to the variable density case. In this work the transmitted waves are measured on a plane parallel to the incident plane wave front, and the experiment is repeated for all view angles. In this scheme, two temporal frequencies are used in the insonifying wave.

The present paper is a generalization of a previous work of the authors (Özbek and Levy, 1987), where the multidimensional inverse scattering problem for a constant density acoustic medium was formulated and solved as a generalized tomographic problem. In this paper, we similarly filter the time traces observed at the receivers to obtain generalized projections of the velocity and density scattering potentials, which are related to the velocity and density variations in the medium. The generalized projections are weighted integrals of the scattering functions; in the two-dimensional geometry the weighting functions are concentrated along parabolas, in the three-dimensional geometry they are concentrated over circular paraboloids. Thus the inverse scattering problem is again posed as a generalized tomographic or

integral geometric problem.

The reconstruction problem for the generalized projections is formulated in a way similar to the problem of x-ray, or straight-line tomography. The solution is expressed as a backprojection operation where we sum the contributions of all projections passing through a given point in space, followed by a two or three dimensional space-invariant filtering operation. In the Fourier domain, the resulting image is a linear combination of the velocity and density scattering potentials, where the coefficients depend on the angle of incidence of the probing wave. Therefore, two or more different angles of incidence are necessary to solve for the velocity and density scattering potentials separately.

The main difference between the approach that we propose here and the diffraction tomography technique developed by Devaney (1985) is that we use *wide-band* plane waves at just a few angles of incidence to reconstruct the medium density and velocity, whereas the diffraction tomography formulation relies on narrowband plane wave sources at just two, and in practice several, frequencies, but *for all angles of incidence*. These two approaches are in some sense dual of each other, since they trade wavevector orientation against frequency. This distinction leads to significantly different processing algorithms, and in fact, as mentioned above, the inversion procedure proposed here is significantly closer to x-ray tomography than to diffraction tomography.

Also, the different choice of experimental conditions appearing here is a reflection of the difference existing between medical imaging applications, which motivated the diffraction tomography approach, and geophysical tomography problems, which are at the origin of the present work. In medical imaging it is possible to rotate the object to be imaged, i.e. the patient, over a 360° range, but in exploration geophysics only a very limited range of angles of incidence can be achieved for surface, or even

vertical seismic profiling recordings.

The paper is organized as follows: we treat the 2-D case in detail in Sections I–III, and just summarize the results for the 3-D case in Section IV. In Section I, the inverse scattering problem is formulated within the Born approximation and redefined as a generalized tomographic problem. The backprojection operation is defined and related to the generalized projections in Section II. In Section III, the separate reconstruction of the velocity and density scattering potentials is discussed. In this context, it is shown that substantially more than two plane-wave experiments are required in order to be able to recover the velocity and density perturbations in a numerically reliable way. We summarize the results for the 3-D geometry in Section IV. A 2-D numerical example is presented in Section V, and Section VI contains some conclusions.

I. PROBLEM DESCRIPTION

In this paper we will treat the two-dimensional case in detail, and summarize the results for the three-dimensional case. Consider the scattering experiment described in Fig. 1. A 2-D acoustic medium is probed by a wide-band plane wave and the scattered field is observed along a straight-line receiver array. The Fourier transform $P(\underline{x}, \omega)$ of the pressure field at point $\underline{x} = (x, y)$ satisfies (Chernov, 1960)

$$\rho(\underline{x}) \nabla \cdot \left[\frac{1}{\rho(\underline{x})} \nabla P(\underline{x}, \omega) \right] + \frac{\omega^2}{c^2(\underline{x})} P(\underline{x}, \omega) = 0, \tag{1}$$

where $c(\underline{x})$ is the propagation velocity, and $\rho(\underline{x})$ is the density of the medium at point $\underline{x}$. The acoustic equation (1) can be rewritten as

$$(\nabla^2 + k^2) P(\underline{x}, \omega) = -k^2 U_c(\underline{x}) P(\underline{x}, \omega) + \nabla U_\rho(\underline{x}) \cdot \nabla P(\underline{x}, \omega), \tag{2}$$

where

$$U_c(\underline{x}) \triangleq \frac{c_o^2}{c^2(\underline{x})} - 1, \tag{3}$$

$$U_\rho(\underline{x}) \triangleq \ln \frac{\rho(\underline{x})}{\rho_o}, \tag{4}$$

and $k = \omega/c_o$ is the wavenumber. Here, $U_c(\underline{x})$ and $U_\rho(\underline{x})$ are respectively called the velocity and the density scattering potentials. c_o and ρ_o are respectively the velocity and the density of the background medium. We assume that $c(\underline{x})$ and $\rho(\underline{x})$ do not deviate significantly from their nominal values c_o and ρ_o; consequently $U_c(\underline{x})$ and $U_\rho(\underline{x})$ are small with respect to 1. We also assume that $U_c(\underline{x})$ and $U_\rho(\underline{x})$ have a bounded support $\mathcal{V}$, which is located completely on one side of the receiver array.

The probing wave $P_o(\underline{x}, \omega)$ satisfies

$$(\nabla^2 + k^2)P_o(\underline{x}, \omega) = 0, \tag{5}$$

so that the scattered field $P_s(\underline{x}, \omega) = P(\underline{x}, \omega) - P_o(\underline{x}, \omega)$ obeys

$$(\nabla^2 + k^2)P_s(\underline{x}, \omega) = -k^2 U_c(\underline{x})P(\underline{x}, \omega) + \nabla U_\rho(\underline{x}) \cdot \nabla P(\underline{x}, \omega). \tag{6}$$

The solution of (6) is given by the Lippmann-Schwinger equation (Taylor, 1972)

$$P_s(\underline{x}, \omega) = \int d\underline{x}' \left[k^2 U_c(\underline{x}')P(\underline{x}', \omega) - \nabla U_\rho(\underline{x}') \cdot \nabla P(\underline{x}', \omega) \right] G_o(\underline{x}, \underline{x}', \omega), \tag{7}$$

where $G_o(\underline{x}, \underline{x}', \omega)$ is the Green's function associated with a point source in a homogeneous medium:

$$(\nabla^2 + k^2)G_o(\underline{x}, \underline{x}', \omega) = -\delta(\underline{x} - \underline{x}'). \tag{8}$$

Equation (7) demonstrates the nonlinear relation that exists between the potentials $U_c(\underline{x})$, $U_\rho(\underline{x})$ and the pressure field $P(\underline{x}, \omega)$. To linearize this equation we adopt the Born approximation, whereby we assume $P_s(\underline{x}, \omega) \ll P_o(\underline{x}, \omega)$. Then the Lippmann-Schwinger equation becomes

$$P_s(\underline{x}, \omega) \approx \int d\underline{x}' \left[k^2 U_c(\underline{x}')P_o(\underline{x}', \omega) - \nabla U_\rho(\underline{x}') \cdot \nabla P_o(\underline{x}', \omega) \right] G_o(\underline{x}, \underline{x}', \omega). \tag{9}$$

The Born approximation assumes that the scattered field $P_s(\underline{x}, \omega)$ is small throughout the volume of the object, which requires that both the magnitude of the scattering potentials U_c and U_ρ be small and that the volume of the region $\mathcal{V}$ be small with respect to the dominant wavelength of the probing wave.

If, instead of the Born approximation one uses the Rytov approximation, the requirement that the size of the scattering region be small can be relaxed (Chernov, 1960; Tatarski, 1961; Devaney, 1981). The Rytov approximation is obtained by representing the total pressure field $P(\underline{x}, \omega)$ in terms of its complex phase and linearizing the resulting Riccati equation satisfied by the phase fluctuation (Devaney, 1985).

On the other hand the Born approximation is more accurate than the Rytov approximation for reflected waves (Beydoun and Tarantola, 1986). For the setup considered in this paper, where the wideband property of the probing wave replaces the large number of view angles available in diffraction tomography, it was shown in Özbek and Levy (1987) that the reflected wave configuration provides the most coverage in the Fourier domain for a bandlimited source. Therefore, we adopt the Born approximation in this paper, although similar results can also be derived for the Rytov approximation.

Next, we simplify the second term in the integrand in equation (9) by using the identity (Norton, 1987)

$$(\nabla U_\rho \cdot \nabla P_o)G_o = \nabla \cdot (U_\rho G_o \nabla P_o) - U_\rho \nabla \cdot (G_o \nabla P_o), \qquad (10)$$

and applying the divergence theorem. Over a surface S located outside the domain $\mathcal{V}$ where the density inhomogeneities are located, we have $U_\rho(\underline{x}) = \ln(\rho(\underline{x})/\rho_o) = 0$, so that

$$\int_{\mathcal{V}} d\underline{x}' \nabla \cdot [U_\rho(\underline{x}')G_o(\underline{x}, \underline{x}', \omega)\nabla P_o(\underline{x}', \omega)]$$

$$= \int_S d\underline{s} U_\rho(\underline{x}')G_o(\underline{x},\underline{x}',\omega)\hat{\underline{n}}(\underline{s}) \cdot \nabla P_o(\underline{x}',\omega)$$

$$= 0. \tag{11}$$

For the second term in equation (10), we have

$$\nabla \cdot (G_o\nabla P_o) = \nabla G_o \cdot \nabla P_o + G_o\nabla^2 P_o = \nabla G_o \cdot \nabla P_o - k^2 G_o P_o. \tag{12}$$

The incident wave is given as

$$P_o(\underline{x}',\omega) = e^{ik\hat{\underline{\theta}} \cdot \underline{x}'}, \tag{13}$$

where $\hat{\underline{\theta}} = (\cos\theta, \sin\theta)$ is the unit vector which indicates the angle of incidence of the plane-wave source. Therefore, within the Born approximation, the scattered field at a receiver point $\underline{\xi}$ is given by

$$\begin{aligned}
P_s(\underline{\xi},\omega) &= \int d\underline{x}' \left\{ k^2[U_c(\underline{x}') - U_\rho(\underline{x}')]P_o(\underline{x}',\omega)G_o(\underline{\xi},\underline{x}',\omega) \right. \\
&\qquad \left. + U_\rho(\underline{x}')\nabla_{\underline{x}'}P_o(\underline{x}',\omega) \cdot \nabla_{\underline{x}'}G_o(\underline{\xi},\underline{x}',\omega) \right\} \\
&= \int d\underline{x}' \left\{ k^2[U_c(\underline{x}') - U_\rho(\underline{x}')]G_o(\underline{\xi},\underline{x}',\omega) \right. \\
&\qquad \left. + ikU_\rho(\underline{x}')[\hat{\underline{\theta}} \cdot \nabla_{\underline{x}'}G_o(\underline{\xi},\underline{x}',\omega)] \right\} P_o(\underline{x}',\omega). \tag{14}
\end{aligned}$$

To compare the far-field scattering patterns that are due to velocity and density perturbations, let us use the far field approximation $k|\underline{x}' - \underline{\xi}| \gg 1$. We find

$$\nabla_{\underline{x}'}G_o(\underline{\xi},\underline{x}',\omega) \approx ik\frac{(\underline{x}' - \underline{\xi})}{|\underline{x}' - \underline{\xi}|}G_o(\underline{\xi},\underline{x}',\omega), \tag{15}$$

which is valid for both the 2-D and 3-D Green's functions. Then (14) becomes

$$P_s(\underline{\xi},\omega) \approx k^2 \int d\underline{x}' \left\{ U_c(\underline{x}') - [1 + \cos\alpha(\underline{\xi},\underline{x}',\hat{\underline{\theta}})]U_\rho(\underline{x}') \right\} G_o(\underline{\xi},\underline{x}',\omega)P_o(\underline{x}',\omega), \tag{16}$$

where $\alpha(\underline{\xi},\underline{x}',\hat{\underline{\theta}})$ is the angle between the vectors $-\hat{\underline{\theta}}$ and $\underline{\xi} - \underline{x}'$. From a physical point of view, $\alpha(\underline{\xi},\underline{x}',\hat{\underline{\theta}})$ is the angle at point $\underline{x}'$ between the ray linking $\underline{x}'$ to the

source, which is specified by vector $-\hat{\underline{\theta}}$ since the incident wave is a plane wave, and the ray linking $\underline{x}'$ to receiver $\underline{\xi}$. Since the background medium is assumed to be constant, these rays are straight lines. The different weights in front of $U_c(\underline{x})$ and $U_\rho(\underline{x})$ in (16) correspond to different scattering patterns which are plotted in Figs. 2a and 2b. As indicated by Fig. 2a, the scattering pattern due to $U_c(\underline{x})$ is that of a monopole, whereas Fig. 2b shows that the scattering pattern due to $U_\rho(\underline{x})$ is that of the sum of a monopole and a dipole. Therefore, the scattering due to density perturbations is most prominent for reflected waves, and least prominent for transmitted ones.

Equation (14) can be written in a slightly different form if we introduce the scattering potential

$$U_\kappa(\underline{x}) \triangleq \ln \frac{\kappa(\underline{x})}{\kappa_o} \tag{17}$$

associated to the compressibility $\kappa(\underline{x}) = 1/c^2(\underline{x})\rho(\underline{x})$. We find

$$U_\kappa(\underline{x}) = \ln \frac{c_o^2}{c^2(\underline{x})} - U_\rho(\underline{x}) \approx U_c(\underline{x}) - U_\rho(\underline{x}) \tag{18}$$

for $c(\underline{x})$ near c_o, as assumed above. Therefore (14) can be written as

$$P_s(\underline{\xi}, \omega) = \int d\underline{x}' \left\{ k^2 U_\kappa(\underline{x}') G_o(\underline{\xi}, \underline{x}', \omega) + ik U_\rho(\underline{x}') [\hat{\underline{\theta}} \cdot \nabla_{\underline{x}'} G_o(\underline{\xi}, \underline{x}', \omega)] \right\} P_o(\underline{x}', \omega), \tag{19}$$

and the objective of this paper will be to solve this integral equation for the compressibility and the density scattering potentials $U_\kappa(\underline{x})$ and $U_\rho(\underline{x})$, or equivalently for $U_\rho(\underline{x})$ and the velocity scattering potential $U_c(\underline{x})$.

For the 2-D geometry under consideration, the Green's function is given by

$$G_o(\underline{x}, \underline{x}', \omega) = \frac{i}{4} H_0^{(1)}(k|\underline{x} - \underline{x}'|), \tag{20}$$

where $H_0^{(1)}(\cdot)$ indicates the Hankel function of order zero and type one. In the following, it will be assumed that the receivers are located along a straight line

perpendicular to the unit vector $\hat{\underline{\phi}} = (\cos\phi, \sin\phi)$ and whose distance from the origin in the direction $\hat{\underline{\phi}}$ is p, as shown in Fig. 1. The position of an arbitrary receiver along this line is therefore given by $\underline{\xi} = p\hat{\underline{\phi}} + \xi\hat{\underline{\phi}}^{\perp}$, where $\hat{\underline{\phi}}^{\perp} = (\sin\phi, -\cos\phi)$ is a unit vector perpendicular to $\hat{\underline{\phi}}$, and ξ is an arbitrary coordinate. Then (19) can be expressed as

$$\frac{2\pi}{k^2}P_s(\underline{\xi},\omega) \triangleq \hat{F}(\xi,k) \triangleq \hat{F}_\kappa(\xi,k) - \hat{F}_\rho(\xi,k), \tag{21}$$

where

$$\hat{F}_\kappa(\xi,k) = \frac{i\pi}{2}\int d\underline{x}' U_\kappa(\underline{x}')e^{ik\hat{\underline{\theta}}\cdot\underline{x}'}H_0^{(1)}(k|\underline{x}' - \underline{\xi}|), \tag{22}$$

$$\begin{aligned}
\hat{F}_\rho(\xi,k) &= \frac{\pi}{2k}\int d\underline{x}' U_\rho(\underline{x}')e^{ik\hat{\underline{\theta}}\cdot\underline{x}'}\left\{\hat{\underline{\theta}}\cdot\nabla_{\underline{x}'}H_0^{(1)}(k|\underline{x}' - \underline{\xi}|)\right\} \\
&= -\frac{\pi}{2}\int d\underline{x}' U_\rho(\underline{x}')e^{ik\hat{\underline{\theta}}\cdot\underline{x}'}\left[\hat{\underline{\theta}}\cdot\frac{(\underline{x}' - \underline{\xi})}{|\underline{x}' - \underline{\xi}|}\right]H_1^{(1)}(k|\underline{x}' - \underline{\xi}|), \tag{23}
\end{aligned}$$

and where $H_1^{(1)}(v) = -dH_0^{(1)}(v)/dv$ is the Hankel function of order 1 and type 1.

We define the inverse Fourier transform of $\hat{F}(\xi,k)$ with respect to k as $g(\xi,r)$:

$$g(\xi,r) \triangleq \frac{1}{2\pi}\int_{-\infty}^{\infty} dk\,\hat{F}(\xi,k)e^{-ikr}; \tag{24}$$

$g_\kappa(\xi,r)$ and $g_\rho(\xi,r)$ are similarly defined as the inverse Fourier transforms of $\hat{F}_\kappa(\xi,k)$ and $\hat{F}_\rho(\xi,k)$, respectively. Taking into account the fact that (see Morse and Feshbach, 1953, pp. 1362–1363)

$$\mathcal{F}^{-1}\left\{\frac{i\pi}{2}H_0^{(1)}(ku)\right\} = \frac{1(r-u)}{\sqrt{r^2 - u^2}}, \tag{25}$$

where $1(\cdot)$ is the unit step function, and the relationship

$$\mathcal{F}^{-1}\left\{-\frac{\pi}{2}H_1^{(1)}(ku)\right\} = \frac{r}{u}\frac{1(r-u)}{\sqrt{r^2 - u^2}} \tag{26}$$

that follows from (25), we find that

$$g(\xi,r) = g_\kappa(\xi,r) - g_\rho(\xi,r), \tag{27}$$

where

$$g_\kappa(\xi, r) = \int d\underline{x}' U_\kappa(\underline{x}') \frac{1(r - \hat{\underline{\theta}} \cdot \underline{x}' - |\underline{x}' - \underline{\xi}|)}{\sqrt{(r - \hat{\underline{\theta}} \cdot \underline{x}')^2 - |\underline{x}' - \underline{\xi}|^2}}, \tag{28}$$

and

$$g_\rho(\xi, r) = \int d\underline{x}' U_\rho(\underline{x}') \left[\hat{\underline{\theta}} \cdot \frac{(\underline{x}' - \underline{\xi})}{|\underline{x}' - \underline{\xi}|} \right] \left[\frac{r - \hat{\underline{\theta}} \cdot \underline{x}'}{|\underline{x}' - \underline{\xi}|} \right] \frac{1(r - \hat{\underline{\theta}} \cdot \underline{x}' - |\underline{x}' - \underline{\xi}|)}{\sqrt{(r - \hat{\underline{\theta}} \cdot \underline{x}')^2 - |\underline{x}' - \underline{\xi}|^2}}. \tag{29}$$

Equation (28) expresses $g_\kappa(\xi, r)$ as a weighted integral of the compressibility scattering potential $U_\kappa(\underline{x})$ where the weighting function is nonzero in a region with parabolic support. The parabola satisfies the equation $r = \hat{\underline{\theta}} \cdot \underline{x} - |\underline{x} - \underline{\xi}|$ where r, $\hat{\underline{\theta}}$ and $\underline{\xi}$ are given and $\underline{x}$ varies. The directrix of this parabola is the line $\hat{\underline{\theta}} \cdot \underline{x} = r$ which is perpendicular to the direction $\hat{\underline{\theta}}$ of incidence of the probing wave, and whose focus is the receiver point $\underline{\xi}$. The weighting function becomes infinite for values of $\underline{x}$ along this parabola, so that the largest contribution to the integral is made by the values of $U_\kappa(\underline{x})$ which lie along the parabola. In some sense, $g_\kappa(\xi, r)$ is a projection of $U_\kappa(\underline{x})$ with respect to a function whose singularities are algebraic and located along a parabola.

In (29), $g_\rho(\xi, r)$ is similarly expressed as a weighted integral of the density scattering potential $U_\rho(\underline{x})$. The weighting function again has a parabolic support, but it contains two additional factors. The first factor, $\hat{\underline{\theta}} \cdot (\underline{x}' - \underline{\xi})/|\underline{x}' - \underline{\xi}|$, is again identified as $\cos \alpha(\underline{\xi}, \underline{x}', \hat{\underline{\theta}})$, where $\alpha(\underline{\xi}, \underline{x}', \hat{\underline{\theta}})$ is the angle between the vectors $-\hat{\underline{\theta}}$ and $\underline{\xi} - \underline{x}'$. The second factor in (29), $(r - \hat{\underline{\theta}} \cdot \underline{x}')/|\underline{x}' - \underline{\xi}|$, is a term which equals unity on the parabolic wavefront of the weighting function, and grows as the focus of the parabola (the receiver point) is approached.

In the following, it will be assumed that the projections $g(\xi, r)$ constitute the data obtained from a single plane-wave scattering experiment. To see why this is

the case, observe from (21) and (24) that

$$g(\xi, r) = -c_o \int_{-\infty}^{\infty} \frac{d\omega}{(i\omega)^2} P_s(\underline{\xi}, \omega) e^{-i\omega r/c_o}. \tag{30}$$

Then since

$$\mathcal{F}\{1(t)\} = \frac{1}{i\omega} + \pi\delta(\omega), \tag{31}$$

and observing from (21) that $P_s(\underline{\xi}, \omega = 0) = 0$, we find that

$$g(\xi, r) = -2\pi c_o \left\{ \int_{-\infty}^{r/c_o} d\tau \int_{-\infty}^{\tau} ds P_s(\underline{\xi}, s) - \frac{1}{2} \int_{-\infty}^{\infty} d\tau \int_{-\infty}^{\tau} ds P_s(\underline{\xi}, s) \right\}. \tag{32}$$

The projections $g(\xi, r)$ are therefore obtained by integrating twice the time domain scattered field $P_s(\underline{\xi}, t)$ observed at ξ, and then subtracting a constant equal to half the value of the double integral at $t = +\infty$. This shows that the knowledge of the observed scattered field $P_s(\underline{\xi}, t)$ for all ξ, t is equivalent to that of projections $g(\xi, r)$ for all ξ, r.

On the basis of the above observations, the inverse scattering problem can be formulated as follows: given the generalized projections

$$\{g(\xi, r) : \quad -\infty < \xi < \infty, \quad -\infty < r < \infty\},$$

we want to reconstruct the scattering potentials $U_\kappa(\underline{x})$ and $U_\rho(\underline{x})$.

II. BACKPROJECTION OPERATION

Proceeding as in the constant density inversion problem treated in Özbek and Levy (1987), the first step of our inversion procedure is to perform a backprojection operation on the projections $g(\xi, r)$. We define it as

$$U_B(\underline{x}) \triangleq \int_{-\infty}^{\infty} d\xi \int_{-\infty}^{\infty} dr g(\xi, r) \frac{1(r - \hat{\underline{\theta}} \cdot \underline{x} - |\underline{x} - \underline{\xi}|)}{\sqrt{(r - \hat{\underline{\theta}} \cdot \underline{x})^2 - |\underline{x} - \underline{\xi}|^2}}. \tag{33}$$

At a given point $\underline{x}$, this operation sums the contributions of $\underline{x}$ to the projections $g(\xi, r)$, as appearing in equations (27)-(29). By performing this backprojection operation for every point in the plane, this gives an image, $U_B(\underline{x})$. $U_B(\underline{x})$ is the analog of the backprojected image obtained in x-ray tomography (Deans, 1983) by summing the line projections passing through a given point.

Our first objective is to relate $U_B(\underline{x})$ to the projections $g(\xi, r)$ in the frequency domain. It can be shown that the 2-D Fourier transform of $U_B(\underline{x})$ is given by (see Özbek and Levy, 1987, Section 3 and Appendix A)

$$\hat{U}_B(\underline{k}) \quad \triangleq \quad \int d\underline{x} U_B(\underline{x}) e^{-i\underline{k}\cdot\underline{x}}$$

$$= \quad \frac{i\pi}{\underline{k}\cdot\hat{\underline{\theta}}} e^{-ip\underline{\lambda}\cdot\hat{\underline{\psi}}/2\underline{k}\cdot\hat{\underline{\theta}}} \hat{g}\left(k_\xi = \frac{\underline{\lambda}\cdot\hat{\underline{\psi}}^\perp}{2\underline{k}\cdot\hat{\underline{\theta}}}, \ k_r = \frac{k^2}{2\underline{k}\cdot\hat{\underline{\theta}}}\right), \quad (34)$$

where

$$\hat{g}(k_\xi, k_r) = \int_{-\infty}^{\infty} d\xi \int_{-\infty}^{\infty} dr g(\xi, r) e^{-i(k_\xi\xi + k_r r)} \quad (35)$$

is the 2-D Fourier transform of $g(\xi, r)$, $\underline{k} = (k_x, k_y)$, $k = |\underline{k}|$, $\underline{\lambda} = (k_x^2 - k_y^2, \ 2k_x k_y)$, $\hat{\underline{\psi}} = (\cos(\theta + \phi), \ \sin(\theta + \phi))$, and $\hat{\underline{\psi}}^\perp = (\sin(\theta + \phi), \ -\cos(\theta + \phi))$.

III. SEPARATE RECONSTRUCTION OF $\hat{U}_c(\underline{k})$ AND $\hat{U}_\rho(\underline{k})$

In this section, we first derive a frequency domain relationship between the projections $g(\xi, r)$ and scattering potentials $U_\kappa(\underline{x})$ and $U_\rho(\underline{x})$, thus obtaining a "Projection Slice Theorem" (Deans, 1983) associated with the problem. Inverting this relationship provides both a frequency domain relationship between $\hat{U}_\kappa(\underline{k})$, $\hat{U}_\rho(\underline{k})$, and $\hat{U}_B(\underline{k})$, and a method for the separate reconstruction of $U_\kappa(\underline{x})$ and $U_\rho(\underline{x})$, or equivalently, of $U_c(\underline{x})$ and $U_\rho(\underline{x})$.

From (27), we have

$$\hat{g}(k_\xi, k_r) = \hat{g}_\kappa(k_\xi, k_r) - \hat{g}_\rho(k_\xi, k_r), \quad (36)$$

where $\hat{\hat{g}}_\kappa(k_\xi, k_r)$ and $\hat{\hat{g}}_\rho(k_\xi, k_r)$ are the 2-D Fourier transforms of $g_\kappa(\xi, r)$ and $g_\rho(\xi, r)$, respectively. Since $g_\kappa(\xi, r) = g(\xi, r)$ for the constant density case, it was shown in (Özbek and Levy, 1987, Section 4 and Appendix B) that $\hat{\hat{g}}_\kappa(k_\xi, k_r)$ can be expressed as

$$\hat{\hat{g}}_\kappa(k_\xi, k_r) = -\frac{i\pi \text{sgn}(k_r)}{\sqrt{k_r^2 - k_\xi^2}}\, e^{i\gamma p \text{sgn}(k_r)\sqrt{k_r^2 - k_\xi^2}}\, \hat{U}_\kappa\left(\underline{k} = k_r\hat{\underline{\theta}} + k_\xi\hat{\underline{\phi}}^\perp + \gamma\text{sgn}(k_r)\sqrt{k_r^2 - k_\xi^2}\,\hat{\underline{\phi}}\right),$$
(37)

for $|k_\xi| \leq |k_r|$, where

$$\hat{U}_\kappa(\underline{k}) = \int d\underline{x}' U_\kappa(\underline{x}') e^{-i\underline{k}\cdot\underline{x}'}$$
(38)

is the 2-D Fourier transform of $U_\kappa(\underline{x})$, and

$$\gamma \triangleq \begin{cases} +1 & \text{if } \underline{x}\cdot\hat{\underline{\phi}} - p > 0 \text{ for all } \underline{x} \in \mathcal{V}, \\ -1 & \text{if } \underline{x}\cdot\hat{\underline{\phi}} - p < 0 \text{ for all } \underline{x} \in \mathcal{V}. \end{cases}$$

γ describes which side of the receiver array the support $\mathcal{V}$ of the inhomogeneities is situated.

We now express $\hat{\hat{g}}_\rho(k_\xi, k_r)$ as a function of the 2-D Fourier transform $\hat{U}_\rho(\underline{k})$ of $U_\rho(\underline{x})$. We first take the Fourier transform of $g_\rho(\xi, r)$ with respect to r:

$$\begin{aligned} \hat{g}_\rho(\xi, k_r) &= \int_{-\infty}^{\infty} dr\, g_\rho(\xi, r) e^{-ik_r r} \\ &= \hat{F}_\rho^{\,*}(\xi, k_r) \\ &= \frac{\pi}{2k_r} \int d\underline{x}' U_\rho(\underline{x}') e^{-ik_r\hat{\underline{\theta}}\cdot\underline{x}'} \left\{ \hat{\underline{\theta}} \cdot \nabla_{\underline{x}'} H_0^{(2)}(k_r|\underline{x}' - \underline{\xi}|) \right\}, \end{aligned}$$
(39)

where $\hat{F}_\rho^{\,*}$ denotes the complex conjugate of $\hat{F}_\rho$ and $H_0^{(2)}(\cdot)$ is the Hankel function of order 0 and type 2. Now, taking the Fourier transform with respect to ξ gives

$$\hat{\hat{g}}_\rho(k_\xi, k_r) = \frac{\pi}{2k_r} \int d\underline{x}' U_\rho(\underline{x}') e^{-ik_r\hat{\underline{\theta}}\cdot\underline{x}'} \left\{ \hat{\underline{\theta}} \cdot \nabla_{\underline{x}'} N(\underline{x}', k_\xi, k_r) \right\},$$
(40)

where (Özbek and Levy, 1987, Appendix B)

$$
N(\underline{x}', k_\xi, k_r) \triangleq \int_{-\infty}^{\infty} d\xi H_0^{(2)}(k_r|\underline{x}' - \underline{\xi}|)e^{-ik_\xi\xi}
$$

$$
= \frac{2\mathrm{sgn}(k_r)}{\sqrt{k_r^2 - k_\xi^2}} e^{-i(k_\xi\underline{x}'\cdot\hat{\underline{\phi}}^\perp + \mathrm{sgn}(k_r)\sqrt{k_r^2 - k_\xi^2}|p-\underline{x}'\cdot\hat{\underline{\phi}}|)} \tag{41}
$$

for $|k_\xi| \leq |k_r|$. Consequently, we get

$$
\hat{\tilde{g}}_\rho(k_\xi, k_r) = -\frac{i\pi}{|k_r|\sqrt{k_r^2 - k_\xi^2}} e^{i\gamma p s\mathrm{gn}(k_r)\sqrt{k_r^2 - k_\xi^2}} \left\{ \hat{\underline{\theta}} \cdot [k_\xi\hat{\underline{\phi}}^\perp + \gamma\mathrm{sgn}(k_r)\sqrt{k_r^2 - k_\xi^2}\,\hat{\underline{\phi}}] \right\}
$$

$$
\cdot\hat{U}_\rho\left(\underline{k} = k_r\hat{\underline{\theta}} + k_\xi\hat{\underline{\phi}}^\perp + \gamma\mathrm{sgn}(k_r)\sqrt{k_r^2 - k_\xi^2}\,\hat{\underline{\phi}}\right), \tag{42}
$$

for $|k_\xi| \leq |k_r|$. Combining (36), (37) and (42), we obtain

$$
\hat{\tilde{g}}(k_\xi, k_r) =
$$
$$
-\frac{i\pi\mathrm{sgn}(k_r)}{\sqrt{k_r^2 - k_\xi^2}} e^{i\gamma p s\mathrm{gn}(k_r)\sqrt{k_r^2 - k_\xi^2}} \left\{ \hat{U}_\kappa\left(\underline{k} = k_r\hat{\underline{\theta}} + k_\xi\hat{\underline{\phi}}^\perp + \gamma\mathrm{sgn}(k_r)\sqrt{k_r^2 - k_\xi^2}\,\hat{\underline{\phi}}\right) \right.
$$
$$
\left. -\frac{\hat{\underline{\theta}} \cdot [k_\xi\hat{\underline{\phi}}^\perp + \gamma\mathrm{sgn}(k_r)\sqrt{k_r^2 - k_\xi^2}\,\hat{\underline{\phi}}]}{k_r} \hat{U}_\rho\left(\underline{k} = k_r\hat{\underline{\theta}} + k_\xi\hat{\underline{\phi}}^\perp + \gamma\mathrm{sgn}(k_r)\sqrt{k_r^2 - k_\xi^2}\,\hat{\underline{\phi}}\right) \right\},
$$
$$
\tag{43}
$$

for $|k_\xi| \leq |k_r|$. For $|k_\xi| > |k_r|$, $\hat{\tilde{g}}(k_\xi, k_r)$ is related to the part of the observed scattered field that corresponds to evanescent waves (Özbek and Levy, 1987), and we do not make use of this portion of $\hat{\tilde{g}}(k_\xi, k_r)$ in our inversion scheme . The inverse formula of (43) is

$$
\hat{U}_R(\underline{k}) \triangleq \hat{U}_c(\underline{k}) - 2\left[\frac{(\underline{k}\cdot\hat{\theta})^2}{k^2}\right]\hat{U}_\rho(\underline{k})
$$

$$
= \frac{i\gamma\underline{\lambda}\cdot\hat{\underline{\psi}}}{2\pi\underline{k}\cdot\hat{\underline{\theta}}} e^{-ip\underline{\lambda}\cdot\hat{\underline{\psi}}/2\underline{k}\cdot\hat{\theta}} \hat{\tilde{g}}\left(k_\xi = \frac{\underline{\lambda}\cdot\hat{\underline{\psi}}^\perp}{2\underline{k}\cdot\hat{\underline{\theta}}}, \ k_r = \frac{k^2}{2\underline{k}\cdot\hat{\underline{\theta}}}\right), \quad \underline{k} \in \mathcal{C}, \tag{44}
$$

where the cone C is defined below, and where $\hat{U}_c(\underline{k}) = \hat{U}_\kappa(\underline{k}) + \hat{U}_\rho(\underline{k})$ is the 2-D Fourier transform of the velocity scattering potential $U_c(\underline{x})$. Here, $\hat{U}_R(\underline{k})$ denotes the 2-D Fourier transform of the reconstructed potential $U_R(\underline{x})$ obtained by applying the constant density reconstruction procedure to the projections $g(\xi, r)$ obtained from a variable density and velocity medium.

Equation (43) represents the "Projection Slice Theorem" associated with the variable density inverse acoustic problem relating the 1-D Fourier transform of $\hat{g}(\xi, k_r)$ with respect to ξ to a semicircular slice of the 2-D Fourier transform of $U_R(\underline{x})$. For a fixed k_r, $\hat{g}(k_\xi, k_r)$ gives $\hat{U}_R(\underline{k})$ along a semicircle of radius $|k_r|$ centered at $k_r \hat{\underline{\theta}}$ as shown in Fig. 3. By letting k_r vary, these semicircles span a cone C, which is defined as

$$C = \{\underline{k} : |\hat{\underline{k}} \cdot \hat{\underline{\nu}}| \geq \sqrt{2}/2\} \tag{45}$$

for $\gamma = +1$, where $\underline{k} = (\hat{\underline{k}}, k)$ and $\hat{\underline{\nu}} = (\cos((\theta + \phi)/2), \sin((\theta + \phi)/2))$. The angular range of this cone is $90°$, as indicated in Fig. 3. For $\gamma = -1$, C is the complement $\bar{C}$ of the above cone.

Combining (34) and (44) gives

$$\hat{U}_R(\underline{k}) = \frac{\gamma \underline{\lambda} \cdot \hat{\psi}}{2\pi^2} \hat{U}_B(\underline{k}) = \hat{U}_c(\underline{k}) - 2\cos^2 \varsigma \, \hat{U}_\rho(\underline{k}), \quad \underline{k} \in C. \tag{46}$$

where ς is the angle between the vectors $\hat{\underline{k}}$ and $\hat{\underline{\theta}}$, with $\underline{k} = (\hat{\underline{k}}, k)$. This relation is the key result of our paper. It shows that the reconstructed image $\hat{U}_R(\underline{k})$ can be obtained by applying the 2-D filter $\gamma \underline{\lambda} \cdot \hat{\psi}/2\pi^2$ to the backprojected image $\hat{U}_B(\underline{k})$. This relation is similar to the identity which is used for 2-D backprojection and filtering x-ray reconstruction methods (Deans, 1983). Since the filter $\underline{\lambda} \cdot \hat{\psi}$ diverges for high frequencies $\underline{k}$, it needs to be "clipped" as $\underline{k}$ becomes large. Furthermore, identity (46) shows that $\hat{U}_R(\underline{k})$ is a linear combination of $\hat{U}_c(\underline{k})$ and $\hat{U}_\rho(\underline{k})$. This implies that it is not possible to reconstruct these two potentials from a single

experiment. To reconstruct $\hat{U}_c(\underline{k})$ and $\hat{U}_\rho(\underline{k})$ separately, we need in principle two experiments with plane waves incident at angles $\hat{\underline{\theta}}_1$ and $\hat{\underline{\theta}}_2$; then we can solve the system

$$\underbrace{\begin{bmatrix} 1 & -2(\hat{\underline{k}} \cdot \hat{\underline{\theta}}_1)^2 \\ 1 & -2(\hat{\underline{k}} \cdot \hat{\underline{\theta}}_2)^2 \end{bmatrix}}_{M(\hat{\underline{k}}; \hat{\underline{\theta}}_1, \hat{\underline{\theta}}_2)} \begin{bmatrix} \hat{U}_c(\underline{k}) \\ \hat{U}_\rho(\underline{k}) \end{bmatrix} = \begin{bmatrix} \hat{U}_{R1}(\underline{k}) \\ \hat{U}_{R2}(\underline{k}) \end{bmatrix}, \tag{47}$$

which requires inverting the matrix $M(\hat{\underline{k}}; \hat{\underline{\theta}}_1, \hat{\underline{\theta}}_2)$.

For the numerical stability and robustness of the matrix inversion procedure, the matrix $M(\hat{\underline{k}}; \hat{\underline{\theta}}_1, \hat{\underline{\theta}}_2)$ must be as nonsingular as possible. The most appropriate measure of the singularity of a matrix is the smallest singular value of the matrix. The smallest singular value of the matrix M is

$$\sigma_{\min}(M) = \min_{i=1,2} \sigma_i \text{ such that } \det(\sigma_i^2 I - M'M) = 0$$

$$= \left\{ 2\eta_1^4 + 2\eta_2^4 + 1 - \left[\left(2\eta_1^4 + 2\eta_2^4 + 1 \right)^2 - 4 \left(\eta_1^2 - \eta_2^2 \right)^2 \right]^{1/2} \right\}^{1/2}, \tag{48}$$

where $\eta_1 \triangleq \hat{\underline{k}} \cdot \hat{\underline{\theta}}_1$ and $\eta_2 \triangleq \hat{\underline{k}} \cdot \hat{\underline{\theta}}_2$.

Inversion of M would be most robust when $\sigma_{\min}(M)$ is maximized. This takes place for values of $\hat{\underline{k}}, \hat{\underline{\theta}}_1$, and $\hat{\underline{\theta}}_2$ such that $\hat{\underline{\theta}}_1 \cdot \hat{\underline{\theta}}_2 = 0$ and $\hat{\underline{k}} = \pm\hat{\underline{\theta}}_1$ or $\hat{\underline{k}} = \pm\hat{\underline{\theta}}_2$. Therefore the two probing waves must be incident at angles perpendicular to each other. Under this condition, let us consider the frequency domain coverage we would have for finite bandwidth data, assuming that we have receiver coverage surrounding the medium. Neglecting the low frequency cutoff band, the frequency domain coverage due to a single probing wave has a "figure-of-eight" shape aligned with the direction of the probing wave (Özbek and Levy, 1987). When two probing waves are used, $U_c(\underline{k})$ and $U_\rho(\underline{k})$ can be solved only in regions where where there is double coverage, as indicated by the shaded areas in Fig. 4. However, if we consider

the superimposed "radiation pattern" of $\sigma_{\min}(M)$ drawn in Fig. 4 also, we see that M is most singular for those values of $\underline{k}$ where we have double coverage.

For general values of $\hat{\underline{\theta}}_1$ and $\hat{\underline{\theta}}_2$ the situation is similar. In general, M is singular for values of $\hat{\underline{k}}$ which satisfy $|\hat{\underline{k}} \cdot \hat{\underline{\theta}}_1| = |\hat{\underline{k}} \cdot \hat{\underline{\theta}}_2|$. Therefore, for $\hat{\underline{\theta}}_1 = \pm\hat{\underline{\theta}}_2$, M is singular for all $\hat{\underline{k}}$; otherwise, it is singular for $\hat{\underline{k}} = \pm(\hat{\underline{\theta}}_1+\hat{\underline{\theta}}_2)/|\hat{\underline{\theta}}_1+\hat{\underline{\theta}}_2|$ or $\hat{\underline{k}} = \pm(\hat{\underline{\theta}}_1-\hat{\underline{\theta}}_2)/|\hat{\underline{\theta}}_1-\hat{\underline{\theta}}_2|$. These are the directions which in fact bisect the regions where there is double coverage. The coverage and radiation pattern for the case when the angle between $\hat{\underline{\theta}}_1$ and $\hat{\underline{\theta}}_2$ is 45° is shown in Fig. 5.

The preceding analysis confirms what researchers in diffraction tomography and exploration geophysics have suspected for some time: namely, that it is exceedingly difficult to reconstruct simultaneously the velocity and density perturbations of an acoustic medium in a numerically stable way. A purely theoretical analysis neglecting the bandlimitation of the probing wave would lead to the conclusion that only two experiments at different angles of incidence are necessary. Yet, as shown above, the numerical results obtained by such an approach would be worthless. In practice, one must use substantially more than two angles of incidence, say angles $\hat{\underline{\theta}}_1, \hat{\underline{\theta}}_2, \ldots, \hat{\underline{\theta}}_N$, and for each $\underline{k}$, solve the resulting system

$$\underbrace{\begin{bmatrix} 1 & -2(\hat{\underline{k}} \cdot \hat{\underline{\theta}}_{i_{\underline{k}1}})^2 \\ 1 & -2(\hat{\underline{k}} \cdot \hat{\underline{\theta}}_{i_{\underline{k}2}})^2 \\ \vdots & \vdots \\ 1 & -2(\hat{\underline{k}} \cdot \hat{\underline{\theta}}_{i_{\underline{k}P}})^2 \end{bmatrix}}_{M(\underline{k})} \begin{bmatrix} \hat{U}_c(\underline{k}) \\ \hat{U}_\rho(\underline{k}) \end{bmatrix} = \underbrace{\begin{bmatrix} \hat{U}_{Ri_{\underline{k}1}}(\underline{k}) \\ \hat{U}_{Ri_{\underline{k}2}}(\underline{k}) \\ \vdots \\ \hat{U}_{Ri_{\underline{k}P}}(\underline{k}) \end{bmatrix}}_{\underline{d}_R(\underline{k})} \tag{49}$$

by the least squares method, where $\{i_{\underline{k}1}, i_{\underline{k}2}, \ldots, i_{\underline{k}P}\} \subset \{1, 2, \ldots, N\}$ is the set of indices corresponding to the angles of incidence for which the probing wave provides

coverage at $\underline{k}$. This gives the solution

$$
\begin{bmatrix} \hat{U}_c(\underline{k}) \\ \hat{U}_\rho(\underline{k}) \end{bmatrix} = (M'M)^{-1}M'\,\underline{d}_R(\underline{k}). \tag{50}
$$

IV. THREE-DIMENSIONAL GEOMETRY

After discussing the 2-D experimental geometry, we summarize the corresponding results for the 3-D case. For the 3-D geometry, we assume that the receivers are on a plane; for convenience we choose this to be the x-y plane. The position of an arbitrary receiver located in this plane is therefore given by $\underline{\xi} = (\underline{\xi}_T, 0)$, where $\underline{\xi}_T$ represents the x-y coordinates of the receiver. The Green's function due to a point source is

$$
G_o(\underline{x}, \underline{x}', \omega) = \frac{e^{ik|\underline{x} - \underline{x}'|}}{4\pi|\underline{x} - \underline{x}'|}. \tag{51}
$$

Under the Born approximation, the Lippmann-Schwinger equation takes the form (19), and the projections in this case become

$$
\begin{aligned}
g(\underline{\xi}_T, r) &= \frac{1}{2\pi}\int_{-\infty}^{\infty} dk\left\{\frac{4\pi}{k^2}P_s(\underline{\xi}, c_o k)\right\}e^{-ikr} \\
&= g_\kappa(\underline{\xi}_T, r) - g_\rho(\underline{\xi}_T, r), \tag{52}
\end{aligned}
$$

where

$$
g_\kappa(\underline{\xi}_T, r) = \int d\underline{x}' U_\kappa(\underline{x}')\frac{\delta(r - \hat{\underline{\theta}}\cdot\underline{x}' - |\underline{x}' - \underline{\xi}|)}{|\underline{x}' - \underline{\xi}|}, \tag{53}
$$

and

$$
g_\rho(\underline{\xi}_T, r) = \int d\underline{x}' U_\rho(\underline{x}')\left[\hat{\underline{\theta}}\cdot\frac{(\underline{x}' - \underline{\xi})}{|\underline{x}' - \underline{\xi}|}\right]\left[\frac{\delta(r - \hat{\underline{\theta}}\cdot\underline{x}' - |\underline{x}' - \underline{\xi}|)}{|\underline{x}' - \underline{\xi}|} + \frac{\mathrm{sgn}(r - \hat{\underline{\theta}}\cdot\underline{x}' - |\underline{x}' - \underline{\xi}|)}{2|\underline{x}' - \underline{\xi}|^2}\right],
$$

$$
\tag{54}
$$

where $\hat{\underline{\theta}}$ is the unit vector in the direction of propagation of the incident wave. The projection $g_\kappa(\underline{\xi}_T, r)$ is again a surface integral of the scattering potential over a circular paraboloid, like in the constant density case. The weighting function appearing in the representation (53) of $g_\kappa(\underline{\xi}_T, r)$ is an impulse, and in this sense the 3-D case is quite different from the 2-D case. Projection $g_\rho(\underline{\xi}_T, r)$ shows further deviations. Like in the 2-D case, it has a cosine dependence on the angle between the direction of the incident wave and the direction of scattering. The weighting function, in addition to an impulse, contains a smoother term which in fact makes $g_\rho(\underline{\xi}_T, r)$ a noncausal function of r. This is due to the $1/k^2$ filter that is applied to the scattered field $P_s(\underline{\xi}, \omega)$ to obtain the projection $g_\rho(\underline{\xi}_T, r)$. If the far-field/high-frequency approximation $k|\underline{x}' - \underline{\xi}| \gg 1$ is made, the impulsive term clearly dominates.

We introduce the backprojection operation as in the constant density case:

$$U_B(\underline{x}) \triangleq \int d\underline{\xi}_T \int_{-\infty}^{\infty} dr g(\underline{\xi}_T, r) \frac{\delta(r - \hat{\underline{\theta}} \cdot \underline{x} - |\underline{x} - \underline{\xi}|)}{|\underline{x} - \underline{\xi}|}. \tag{55}$$

In the frequency domain, the backprojected image can be related to the parabolical projections as (see Özbek and Levy, 1987, Section 8 and Appendix C)

$$\hat{U}_B(\underline{k}) = \frac{i2\pi}{\underline{k} \cdot \hat{\underline{\theta}}} \hat{\hat{g}}\left(\underline{k}_{\xi T} = \left(\frac{\underline{\lambda}_x \cdot \hat{\underline{\theta}}}{2\underline{k} \cdot \hat{\underline{\theta}}}, \frac{\underline{\lambda}_y \cdot \hat{\underline{\theta}}}{2\underline{k} \cdot \hat{\underline{\theta}}}\right), \; k_r = \frac{k^2}{2\underline{k} \cdot \hat{\underline{\theta}}}\right), \tag{56}$$

where

$$\hat{U}_B(\underline{k}) \triangleq \int d\underline{x} U_B(\underline{x}) e^{-i\underline{k} \cdot \underline{x}} \tag{57}$$

$$\hat{\hat{g}}(\underline{k}_{\xi T}, k_r) \triangleq \int d\underline{\xi}_T \int_{-\infty}^{\infty} dr g(\underline{\xi}_T, r) e^{-i(\underline{k}_{\xi T} \cdot \underline{\xi}_T + k_r r)}, \tag{58}$$

are the 3-D Fourier transforms of $U_B(\underline{x})$ and $g(\underline{\xi}_T, r)$, and

$$\underline{\lambda}_x \triangleq (k_x^2 - k_y^2 - k_z^2, \; 2k_x k_y, \; 2k_x k_z),$$

$$\underline{\lambda}_y \triangleq (2k_x k_y, \; k_y^2 - k_x^2 - k_z^2, \; 2k_y k_z).$$

From (52), we again have

$$\hat{\hat{g}}(\underline{k}_{\xi T}, k_r) = \hat{\hat{g}}_\kappa(\underline{k}_{\xi T}, k_r) - \hat{\hat{g}}_\rho(\underline{k}_{\xi T}, k_r), \tag{59}$$

where $\hat{\hat{g}}_\kappa(\underline{k}_{\xi T}, k_r)$ and $\hat{\hat{g}}_\rho(\underline{k}_{\xi T}, k_r)$ are the 3-D Fourier transforms of $g_\kappa(\underline{\xi}_T, r)$ and $g_\rho(\underline{\xi}_T, r)$, respectively. Again, since $g_\kappa(\underline{\xi}_T, r) = g(\underline{\xi}_T, r)$ for the constant density case, it was shown in (Özbek and Levy, 1987, Section 8 and Appendix D) that $\hat{\hat{g}}_\kappa(\underline{k}_{\xi T}, k_r)$ takes the form

$$\hat{\hat{g}}_\kappa(\underline{k}_{\xi T}, k_r) = -\frac{i2\pi\,\mathrm{sgn}(k_r)}{\sqrt{k_r^2 - |\underline{k}_{\xi T}|^2}} \hat{U}_\kappa\left(\underline{k} = k_r\underline{\hat{\theta}} + (\underline{k}_{\xi T}, \gamma\mathrm{sgn}(k_r)\sqrt{k_r^2 - |\underline{k}_{\xi T}|^2})\right), \tag{60}$$

for $|\underline{k}_{\xi T}| \leq |k_r|$, where $\hat{U}_\kappa(\underline{k})$ is the 3-D Fourier transform of $U_\kappa(\underline{x})$, and

$$\gamma \triangleq \begin{cases} +1 & \text{if } z > 0 \text{ for all } \underline{x} \in \mathcal{V}, \\ -1 & \text{if } z < 0 \text{ for all } \underline{x} \in \mathcal{V}. \end{cases}$$

Using the intermediate results derived in (Özbek and Levy, 1987, Appendix D), we also have

$$\hat{\hat{g}}_\rho(\underline{k}_{\xi T}, k_r) = -\frac{i2\pi}{|k_r|\sqrt{k_r^2 - |\underline{k}_{\xi T}|^2}} \left[\underline{\hat{\theta}} \cdot (\underline{k}_{\xi T}, \gamma\mathrm{sgn}(k_r)\sqrt{k_r^2 - |\underline{k}_{\xi T}|^2})\right]$$
$$\cdot \hat{U}_\rho\left(\underline{k} = k_r\underline{\hat{\theta}} + (\underline{k}_{\xi T}, \gamma\mathrm{sgn}(k_r)\sqrt{k_r^2 - |\underline{k}_{\xi T}|^2})\right), \tag{61}$$

for $|\underline{k}_{\xi T}| \leq |k_r|$, where $\hat{U}_\rho(\underline{k})$ is the 3-D Fourier transform of $U_\rho(\underline{x})$.

Combining (52), (59) and (60) yields

$$\hat{\hat{g}}(\underline{k}_{\xi T}, k_r) =$$
$$-\frac{i2\pi\mathrm{sgn}(k_r)}{\sqrt{k_r^2 - |\underline{k}_{\xi T}|^2}} \left\{ \hat{U}_\kappa\left(\underline{k} = k_r\underline{\hat{\theta}} + (\underline{k}_{\xi T}, \gamma\mathrm{sgn}(k_r)\sqrt{k_r^2 - |\underline{k}_{\xi T}|^2})\right) \right.$$
$$\left. -\frac{\underline{\hat{\theta}} \cdot (\underline{k}_{\xi T}, \gamma\mathrm{sgn}(k_r)\sqrt{k_r^2 - |\underline{k}_{\xi T}|^2})}{k_r} \hat{U}_\rho\left(\underline{k} = k_r\underline{\hat{\theta}} + (\underline{k}_{\xi T}, \gamma\mathrm{sgn}(k_r)\sqrt{k_r^2 - |\underline{k}_{\xi T}|^2})\right) \right\}, \tag{62}$$

for $|\underline{k}_{\xi T}| \leq |k_r|$.

The inverse formula of (61) is

$$
\begin{aligned}
\hat{U}_R(\underline{k}) &\triangleq \hat{U}_c(\underline{k}) - 2 \left[\frac{(\underline{k} \cdot \hat{\underline{\theta}})^2}{k^2} \right] \hat{U}_\rho(\underline{k}) \\
&= \frac{i\gamma\underline{\lambda}_z \cdot \hat{\underline{\theta}}}{4\pi\underline{k} \cdot \hat{\underline{\theta}}} \, \hat{g}\left(\underline{k}_{\xi T} = \left(\frac{\underline{\lambda}_x \cdot \hat{\underline{\theta}}}{2\underline{k} \cdot \hat{\underline{\theta}}}, \frac{\underline{\lambda}_y \cdot \hat{\underline{\theta}}}{2\underline{k} \cdot \hat{\underline{\theta}}} \right), \; k_r = \frac{k^2}{2\underline{k} \cdot \hat{\underline{\theta}}} \right), \quad \underline{k} \in \mathcal{C},
\end{aligned}
$$

(63)

where

$$
\underline{\lambda}_z \triangleq (2k_x k_z, \; 2k_y k_z, \; k_z^2 - k_x^2 - k_y^2),
$$

and where $\hat{U}_c(\underline{k}) = \hat{U}_\kappa(\underline{k}) + \hat{U}_\rho(\underline{k})$ is the 3-D Fourier transform of the velocity scattering potential $U_c(\underline{x})$. Here, $\hat{U}_R(\underline{k})$ denotes the 3-D Fourier transform of the reconstructed potential $U_R(\underline{x})$ which is obtained by applying the constant density reconstruction procedure to the projections $g(\underline{\xi}_T, r)$ obtained from a variable density and velocity medium.

For $|\underline{k}_{\xi T}| > |k_r|$, as in the 2-D case, $\hat{\hat{g}}(\underline{k}_{\xi T}, k_r)$ is related to the part of the observed scattered field that corresponds to evanescent waves, and we do not make use of this portion of $\hat{\hat{g}}(\underline{k}_{\xi T}, k_r)$ in our inversion scheme.

Equation (61) represents the "Projection Slice Theorem" for the 3-D case associated with the variable density inverse acoustic problem. For a fixed k_r, the 2-D Fourier transform of $\hat{g}(\underline{\xi}_T, k_r)$ gives the 3-D Fourier transform of $U_R(\underline{x})$ over a hemisphere of radius $|k_r|$ centered at $k_r\hat{\underline{\theta}}$. By letting k_r vary, $\hat{U}(\underline{k})$ is determined in a cone $\mathcal{C}$, which again covers half of the 3-D frequency space.

Combining (56) and (62) gives

$$
\hat{U}_R(\underline{k}) = \frac{\gamma\underline{\lambda}_z \cdot \hat{\underline{\theta}}}{8\pi^2} \hat{U}_B(\underline{k}) = \hat{U}_c(\underline{k}) - 2\cos^2\varsigma \, \hat{U}_\rho(\underline{k}), \quad \underline{k} \in \mathcal{C}.
$$

(64)

Therefore, $\hat{U}_R(\underline{k})$ for $\underline{k} \in C$ can be obtained from $\hat{U}_B(\underline{k})$ by a 3-D space invariant filtering operation.

$\hat{U}_R(\underline{k})$ is related to $\hat{U}_c(\underline{k})$ and $\hat{U}_\rho(\underline{k})$ with the same relationship ((46) and (64)) in two and three dimensions. Therefore, the procedure for individual reconstruction of $U_c(\underline{x})$ and $U_\rho(\underline{x})$ is the same in these two cases.

V. NUMERICAL EXAMPLE

The theory presented in this paper was tested for the two-dimensional case, using computer-generated synthetic data. Figs. 6 and 7 show the velocity and density scattering potential models, $U_c(\underline{x})$ and $U_\rho(\underline{x})$, respectively. The scattering potentials correspond to velocity and density anomalies which are constant in square-shaped areas of dimensions 35 m × 35 m. The background medium was homogeneous with a velocity of 5000 m/s and a density of 2000 kg/m³. The magnitude of the velocity and density perturbations were 10% of the nominal values. A lowpass source wavelet with a cutoff frequency of 425 Hz was used, so that the object sizes are three times the shortest wavelength in the source signal. The regions of anomaly are separated by a distance equal to six times the shortest wavelength. The synthetic scattered waves were obtained by using the forward scattering equation under the Born approximation; however, since the velocity and density perturbations are of limited size with respect to the shortest wavelength, and the magnitudes of these perturbations are relatively small, we do not feel that the approximation is critical for this particular example. The entire image area was 500 m × 500 m, the grid size was 5 m × 5 m, and receivers were located on all sides around the medium, 100 on each side.

As indicated in Section III of this paper, in order to guarantee the numerical stability of the procedure for reconstructing separately the velocity and density'

inhomogeneities, more than two sources are needed. In this experiment, we have used eight angles of incidence, at 22.5° intervals. The inversion was performed over the regions in the $\underline{k}$ domain where coverage was provided by at least five probing waves; i.e., using the notation of eq. (49), $N = 8$, $P \geq 5$, and rank(M) ≥ 4 for all inversion points $\underline{k}$. This corresponds to carrying out the inversion over a circular lowpass region with a radius of about 55% of the maximum frequency coverage provided by a single source.

For comparison, we first examine images $U_B^{av}(\underline{x})$ and $U_R^{av}(\underline{x})$. To obtain these images, in the frequency domain, values obtained due to different sources providing multiple coverage were simply averaged point by point. Fig. 8 shows the back-projected image $U_B^{av}(\underline{x})$. $U_B^{av}(\underline{x})$ can be interpreted as a "migrated" image of the velocity field for a constant density medium (for migration, see, for example, Claerbout, 1985). Fig. 9 depicts $U_R^{av}(\underline{x})$, which is the image obtained by applying the constant density reconstruction procedure to the data obtained from a variable density and velocity medium.

Some observations can be made regarding these images. Both images display the locations of the scatterers; however the "inversion" image is much better focused than the "migration" image. This effect has also been noted by other researchers (Esmersoy and Miller, 1987). In addition, the values of $U_B^{av}(\underline{x})$ differ by orders of magnitude from the numerical values of the true scattering potentials. On the other hand, $U_R^{av}(\underline{x})$ looks like $U_c(\underline{x}) - U_\rho(\underline{x})$, and actual constructed values confirm this. To interpret this result, observe from (46) that, for the "ideal case" where plane wave experiments are performed for all angles θ of incidence, the averaging scheme described above for combining the reconstructed images obtained for different probing

angles can be written as

$$\hat{U}_R^{av}(\underline{k}) = \frac{1}{\pi} \int_0^\pi d\theta \hat{U}_R(\underline{k}) = \hat{U}_c(\underline{k}) - \hat{U}_\rho(\underline{k}) = \hat{U}_\kappa(\underline{k}), \qquad (65)$$

where $\hat{U}_R$ corresponds to the inversion result for one source, and $\hat{U}_R^{av}$ corresponds to the result after angular averaging. Therefore, averaging the reconstructed potential $\hat{U}_R(\underline{k})$ over different angles is equivalent to reconstructing the compressibility potential of the medium.

Figs. 10 and 11 show the separate reconstructions of $U_c(\underline{x})$ and $U_\rho(\underline{x})$, respectively. The numerical values obtained are within 20% of the model values. There exist several sources of error. The first of these is the bilinear interpolation procedure which is used to convert the discretized 2-D Fourier transform $\hat{g}(k_\xi, k_r)$ of the projections into the discretized Fourier transform $\hat{U}_R(\underline{k})$ of the reconstructed image. A second source of error is the fact that all the inversion results developed in this paper assume that receiver arrays are infinite, whereas the arrays which are used for the present example have a finite length. Other errors are due to the fact that the source wavelet is bandlimited, and needs to be deconvolved.

Finally, the DC levels of the velocity and density scattering potentials cannot be reconstructed separately with the derived inversion formulas, since the coefficient of $\hat{U}_\rho(\underline{k})$ in equation (44) is not analytic around $\underline{k} = \underline{0}$. The DC level of $U_\kappa(\underline{x})$ can be recovered from equation (22), so that if the DC level of either the density or the velocity is known, the other one can be computed. In our implementation, we have estimated $U_c(\underline{k} = 0)$ and $U_\rho(\underline{k} = 0)$ as a weighted average of the closest eight values in the discrete wavenumber domain. Adopting the reciprocal of the square of the distance as the measure of weight, we assigned a weight of 1/6 to the closest four samples, and 1/12 to the next closest samples which are diagonally located.

VI. CONCLUSIONS

In this paper we have considered the problem of the reconstructing separately of the velocity and density inhomogeneities of a multidimensional acoustic medium probed by wide-band plane waves. The problem was posed as a generalized tomographic problem, where weighted integrals of the velocity and density scattering potentials $U_c(\underline{x})$ and $U_\rho(\underline{x})$ are used as data. A backprojection operator $U_B(\underline{x})$ was defined, which was related to the generalized projections in the Fourier transform domain. It was shown that, by applying a time-invariant filter to $U_B(\underline{x})$, we can obtain an image, $U_R(\underline{x})$, which in the Fourier domain is a linear combination of the velocity and density scattering potentials, and where the coefficients depend on the angle of incidence of the probing wave. Therefore, for numerical stability, several angles of incidence were used to solve for the velocity and density scattering potentials separately.

ACKNOWLEDGEMENTS

REFERENCES

G. Beylkin and R. Burridge (1987). "Multiparameter Inversion for Acoustic and Elastic Media," presented at the 57th Ann. Int. Mtg. and Expos., Soc. Explor. Geophys., New Orleans, Expanded Abstracts, 747–749.

W. B. Beydoun and A. Tarantola (1986). "First Born and Rytov Approximations: Modeling and Inversion Conditions in a Canonical Example," submitted to J. Acoust. Soc. Am.

L. A. Chernov (1960). *Wave Propagation in a Random Medium* (Dover, New York).

J. F. Claerbout (1985). *Imaging the Earth's Interior* (Blackwell, Oxford).

R. W. Clayton and R. H. Stolt (1981). "A Born-WKBJ Inversion Method for Acoustic Reflection Data," Geophysics **46**, 1559–1567.

S. Coen (1981). "Density and Compressibility Profiles of a Layered Acoustic Medium from Precritical Incidence Data," Geophysics **46**, 1244–1246.

S. Coen, M. Cheney, A. Weglein (1984). "Velocity and Density of a Two-Dimensional Acoustic Medium from Point source Surface Data," J. Math. Phys. **25**, 1857–1861.

S. R. Deans (1983). *The Radon Transform and Some of its Applications* (Wiley Interscience, New York).

A. J. Devaney (1981). "Inverse Scattering Theory within the Rytov Approximation," Opt. Lett. **6**, 374–376.

A. J. Devaney (**1985**). "Variable Density Acoustic Tomography," J. Acoust. Soc. Am. **78**, 374–376.

C. Esmersoy and D. Miller (**1987**). "Stacking Versus Back Propagation in Seismic Imaging: Duality for Multidimensional Linearized Inversion," presented at the 57th Ann. Int. Mtg. and Expos., Soc. Explor. Geophys., New Orleans, Expanded Abstracts, 744–746.

M. A. Hooshyar and M. Razavy (**1983**). "A Method for Constructing Wave Velocity and Density Profiles from the Angular Dependence of the Reflection Coefficient," J. Acoust. Soc. Am. **73**, 19–23.

M. A. Hooshyar and A. B. Weglein (**1986**). "Inversion of the Two-Dimensional SH Elastic Wave Equation for the Density and Shear Modulus," J. Acoust. Soc. Am. **79**, 1280–1283.

P. M. Morse and H. Feshbach (**1953**). *Methods of Theoretical Physics* (McGraw-Hill, New York).

S. J. Norton (**1983**). "Generation of Separate Density and Compressibility Images in Tissue," Ultrasonic Imaging **5**, 240–252.

S. J. Norton (**1987**). "Three-Dimensional Seismic Inversion of Velocity- and Density-Dependent Reflectivity," Geophys. J. R. Astr. Soc. **88**, 393–415.

A. Özbek and B. C. Levy (**1987**). "Inversion of Parabolic and Paraboloidal Projections," Report LIDS-P-1665, Laboratory for Information and Decision Systems, Mass. Inst. of Tech., Cambridge, MA; see also Proc. 21st Conf. Information Sciences and Systems, The Johns Hopkins Univ., Baltimore, MD, 36–42.

A. G. Ramm and A. B. Weglein (**1984**). "Inverse Scattering for Geophysical Problems. II. Inversion of Acoustical Data," J. Math. Phys. **25** 3231–3234.

S. Raz (**1981a**). "Direct Reconstruction of Velocity and Density Profiles from Scattered Field Data," Geophysics **46**, 832–836.

S. Raz (**1981b**). "Three-Dimensional Velocity Profile Inversion from Finite-Offset Scattering Data," Geophysics **46**, 837–842.

V. T. Tatarski (**1961**). *Wave Propagation in a Turbulent Medium* (McGraw-Hill, New York).

J. R. Taylor (**1972**). *Scattering Theory* (John Wiley, New York).

A. E. Yagle and B. C. Levy (**1984**). "Application of the Schur Algorithm to the Inverse Problem for a Layered Acoustic Medium," J. Acoust. Soc. Am. **76**, 301–308.

Figure Captions

Fig. 1 2-D experimental geometry.

Fig. 2a Scattering pattern due to velocity inhomogeneities.

Fig. 2b Scattering pattern due to density inhomogeneities.

Fig. 3 Coverage of $\hat{U}_R(\underline{k})$ for a single array.

Fig. 4 Frequency coverage of $\hat{U}_R(\underline{k})$ and the "radiation pattern" of $\sigma_{\min}(M; \hat{\underline{k}}; \hat{\theta}_1, \hat{\theta}_2)$ for the case when two probing waves are used, incident at right angles to each other.

Fig. 5 Frequency coverage when of $\hat{U}_R(\underline{k})$ and the "radiation pattern" of $\sigma_{\min}(M; \hat{\underline{k}}; \hat{\theta}_1, \hat{\theta}_2)$ for the case when two probing waves are used, incident at a 45° angle with respect to each other.

Fig. 6 Velocity scattering potential model for the synthetic experiment.

Fig. 7 Density scattering potential model for the synthetic experiment.

Fig. 8 The backprojected image $U_B^{av}(\underline{x})$, obtained assuming a constant density medium.

Fig. 9 The inverted image $U_R^{av}(\underline{x})$, obtained assuming a constant density medium.

Fig. 10 The separate reconstruction of the velocity scattering potential.

Fig. 11 The separate reconstruction of the density scattering potential.
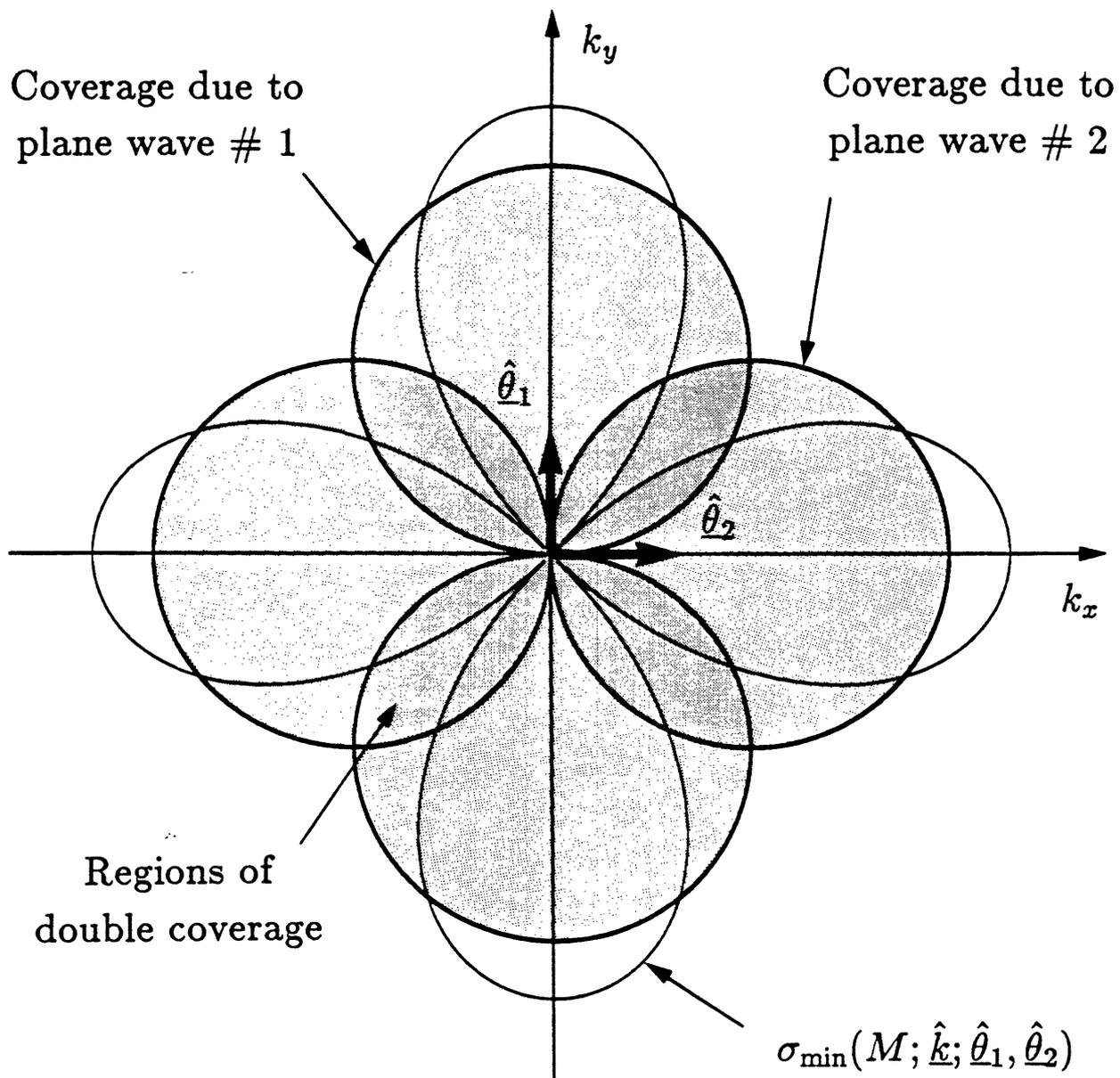
Fig. 1

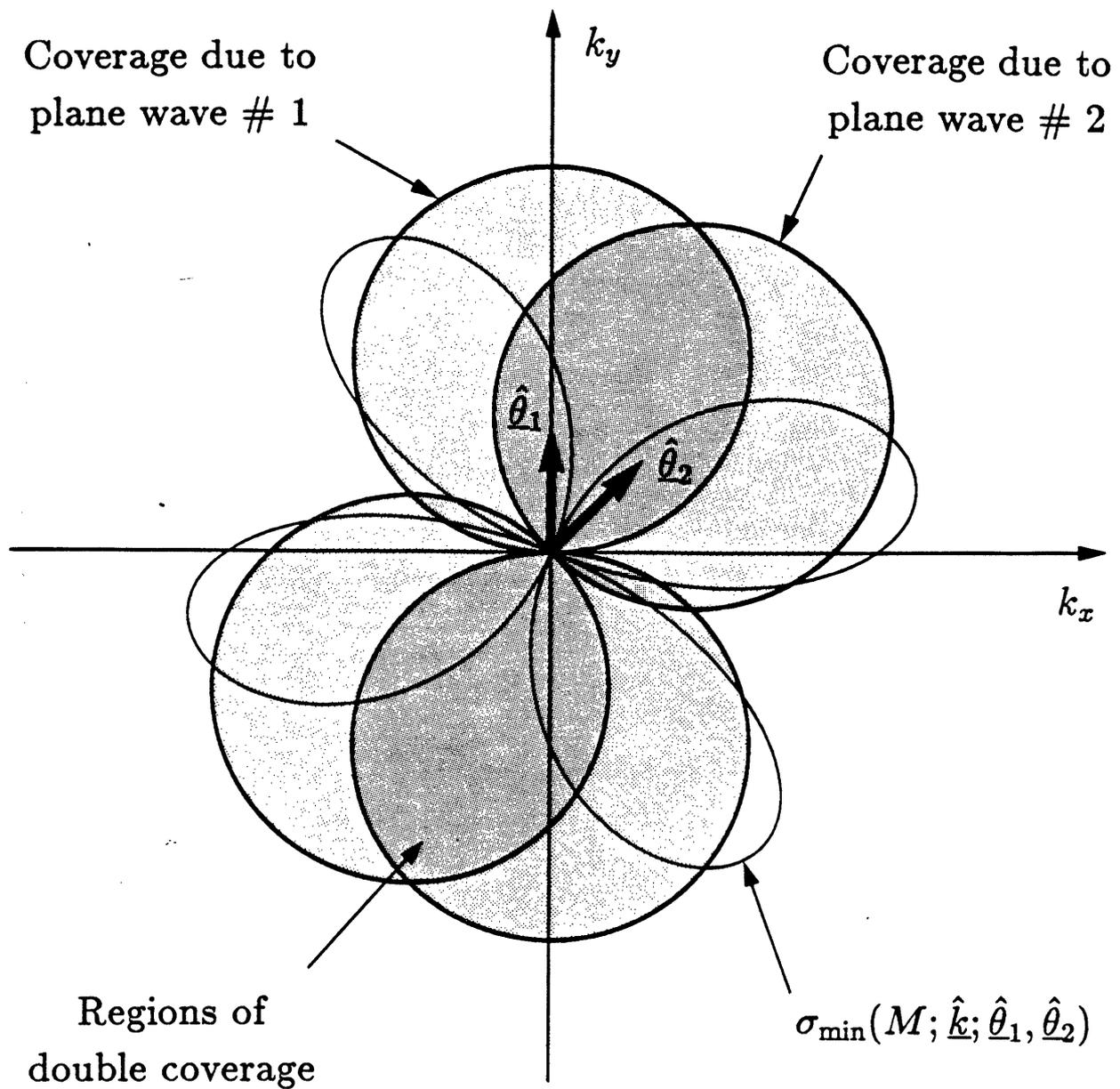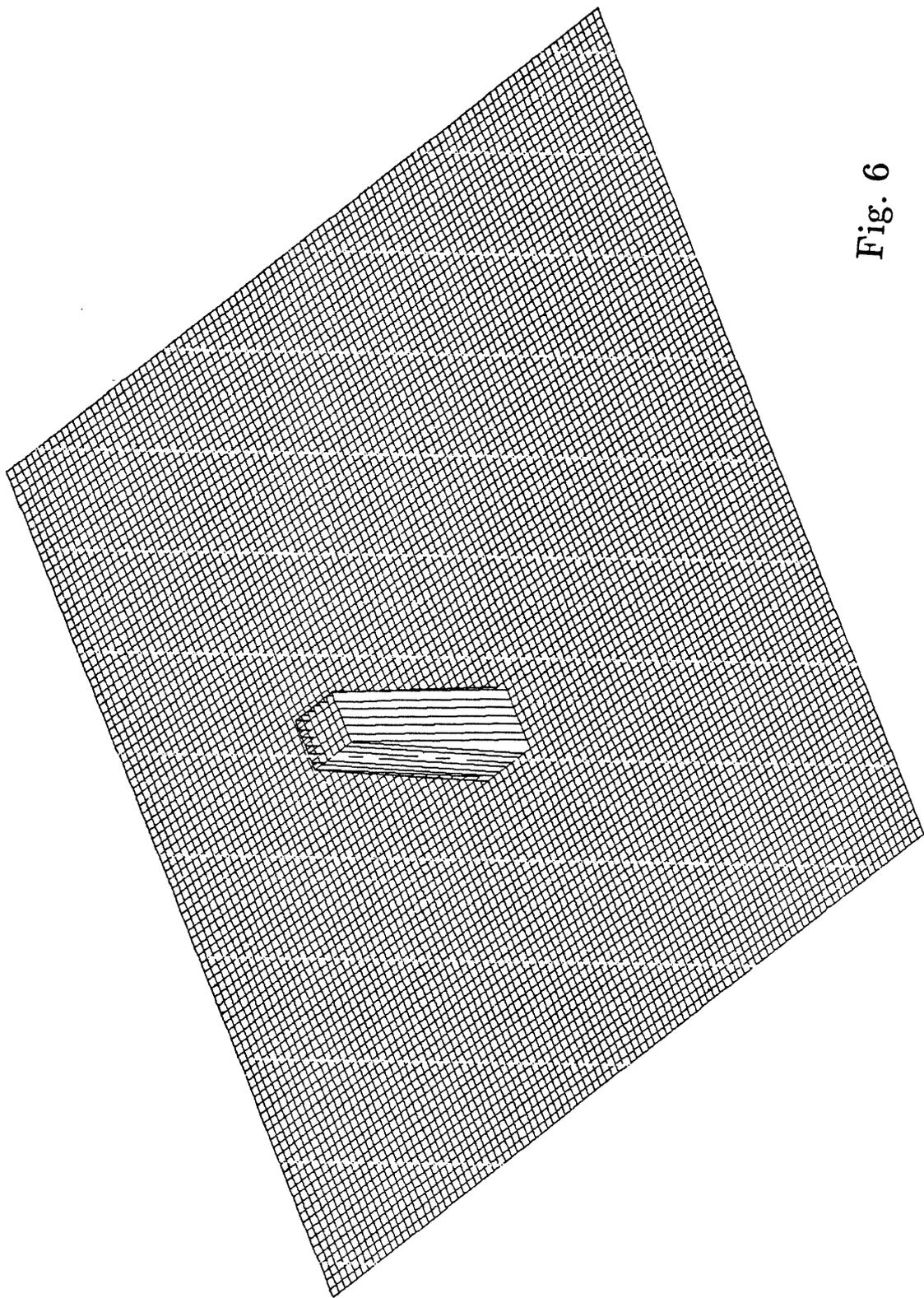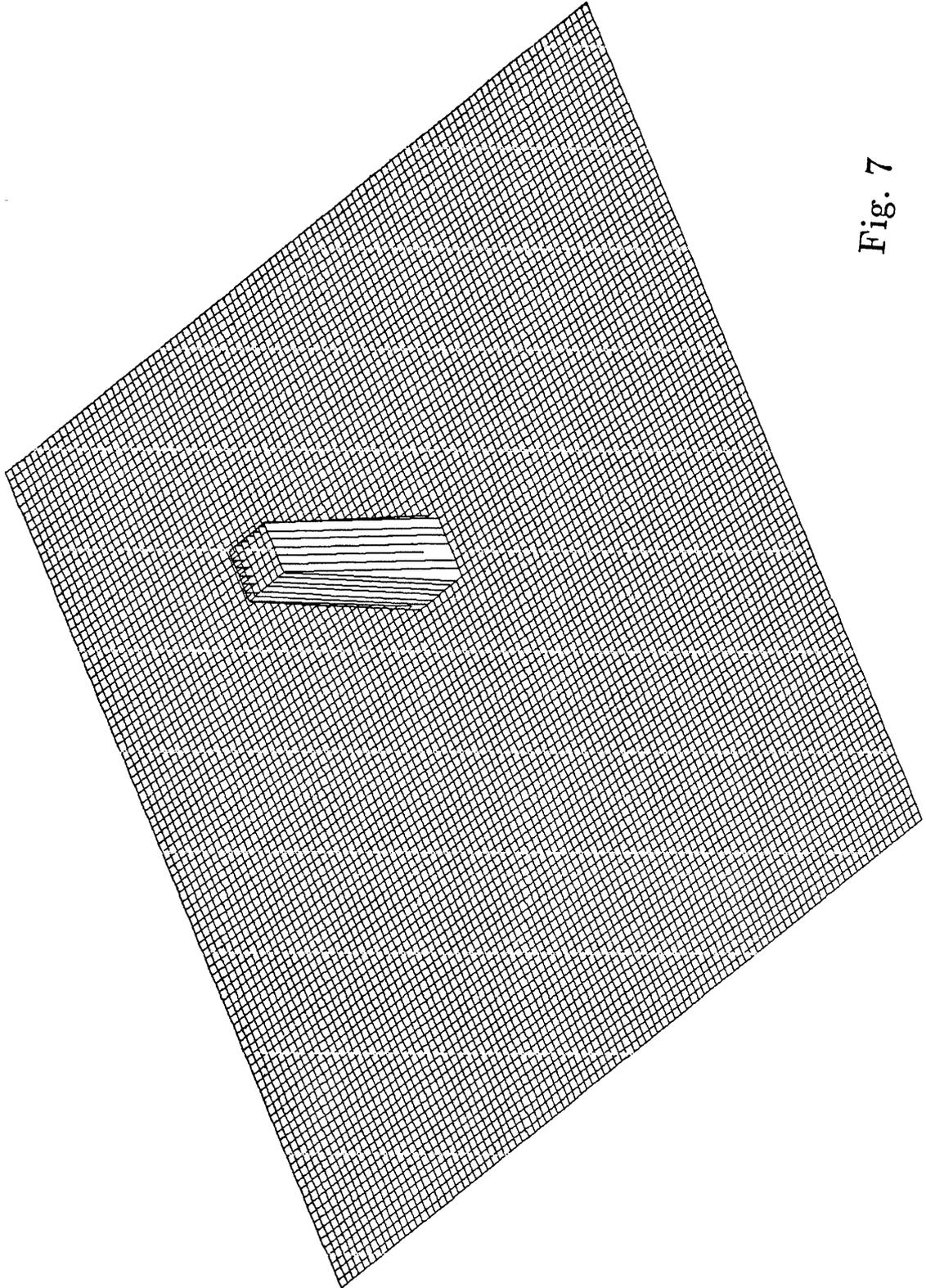$\hat{\underline{\theta}}$

(a)

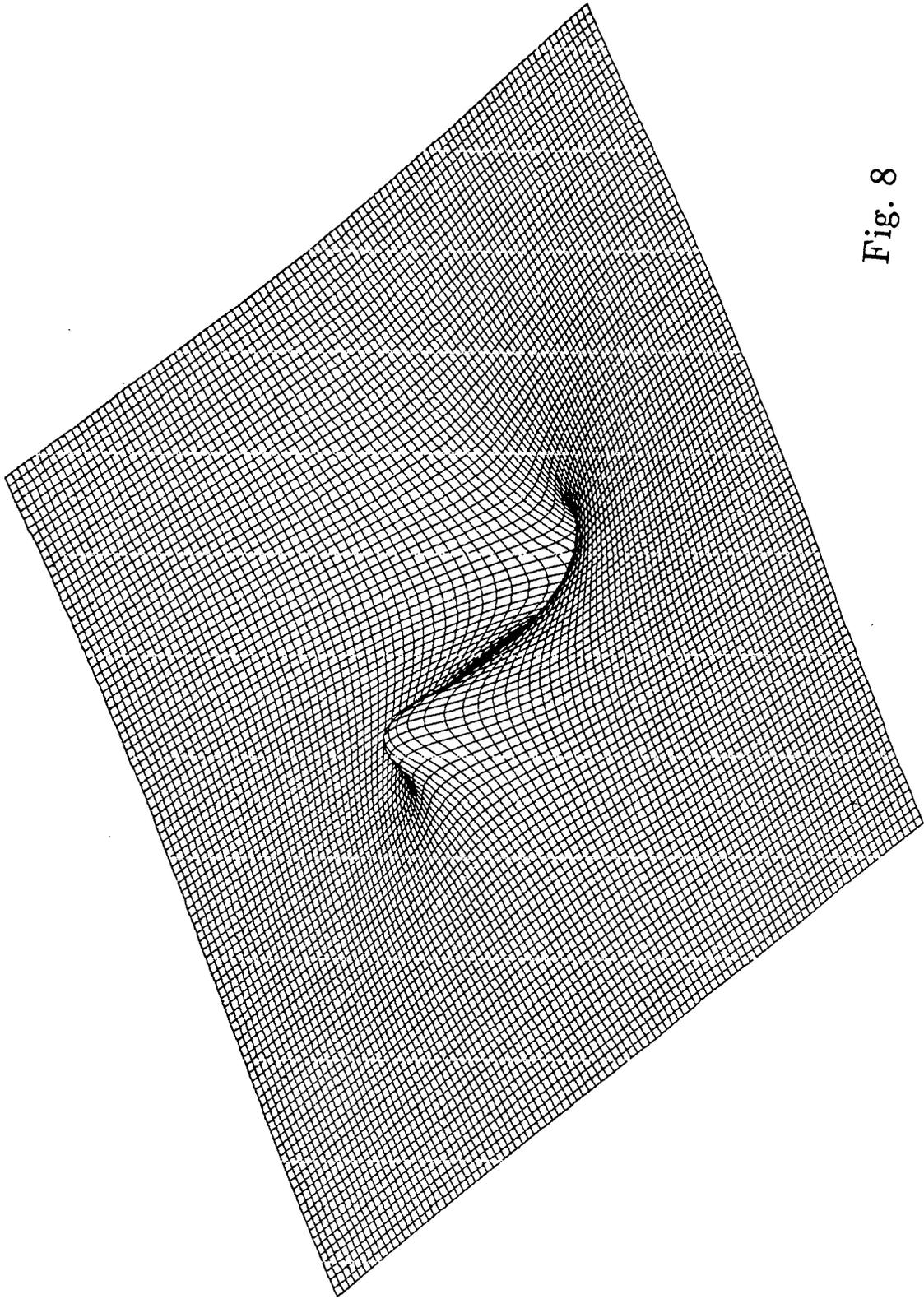$\hat{\underline{\theta}}$

(b)
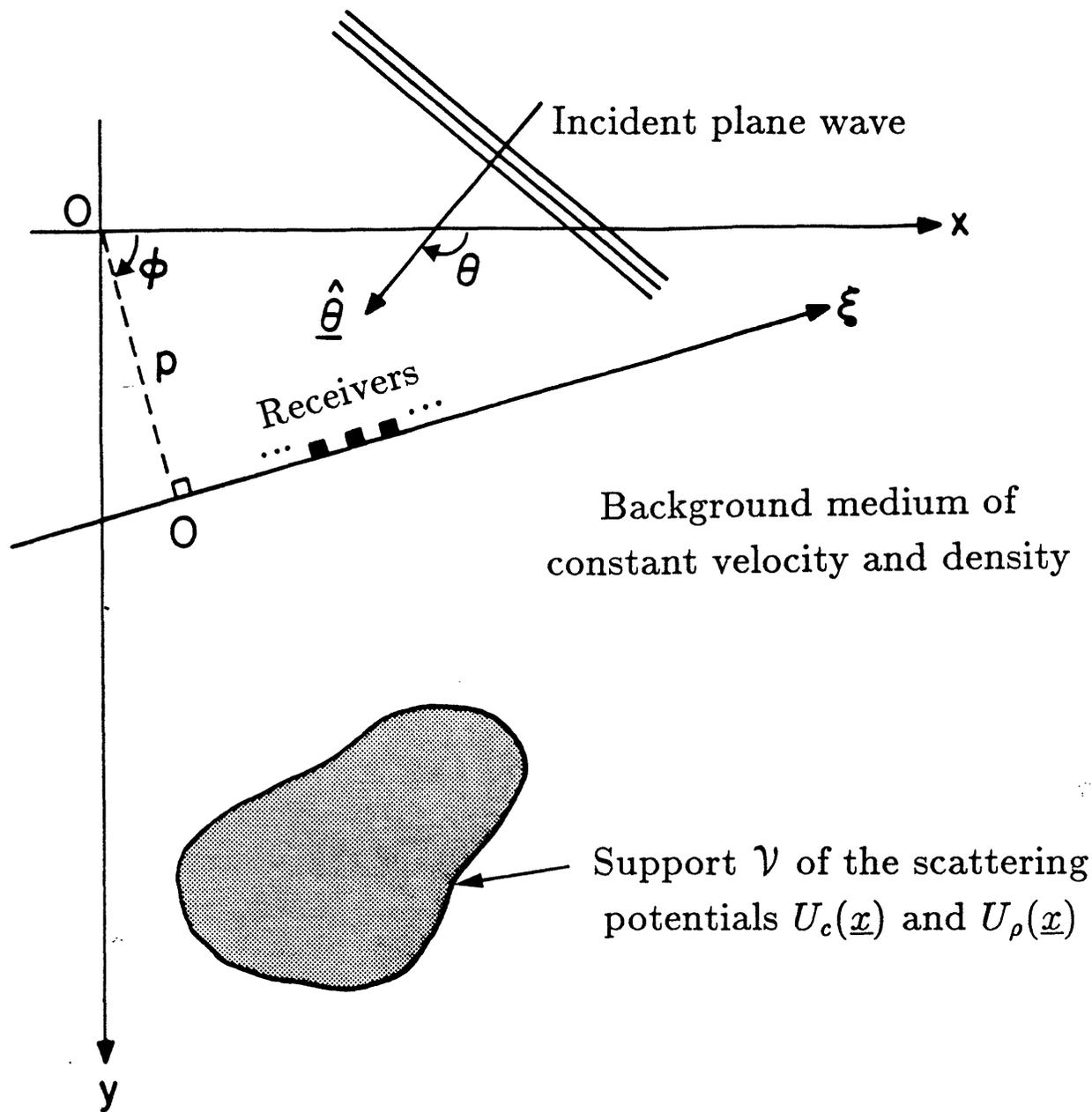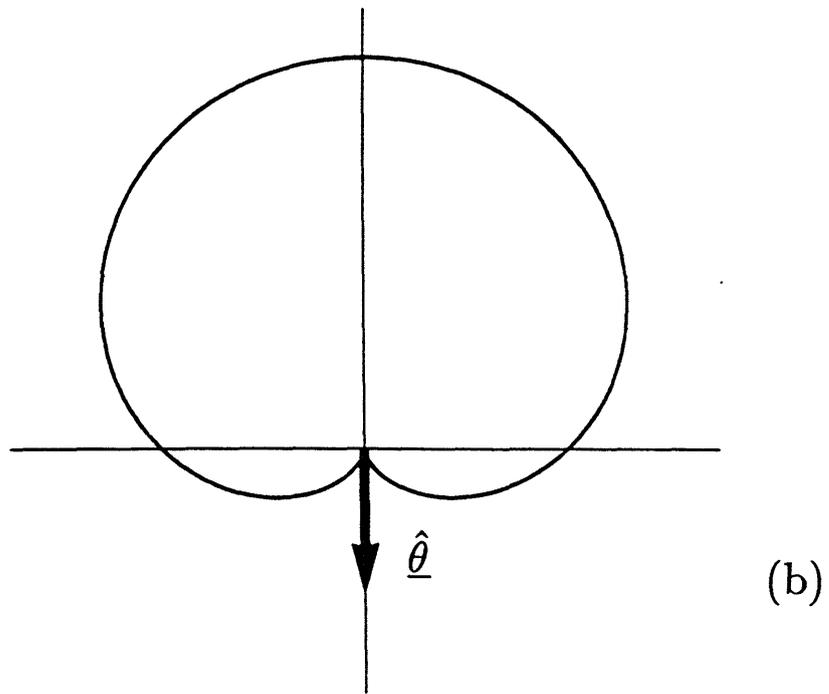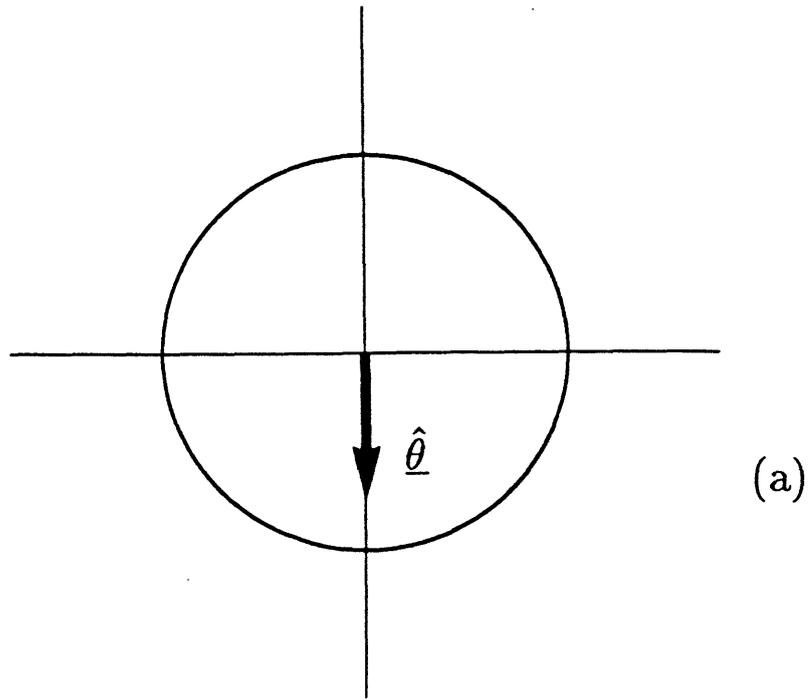
Fig. 2
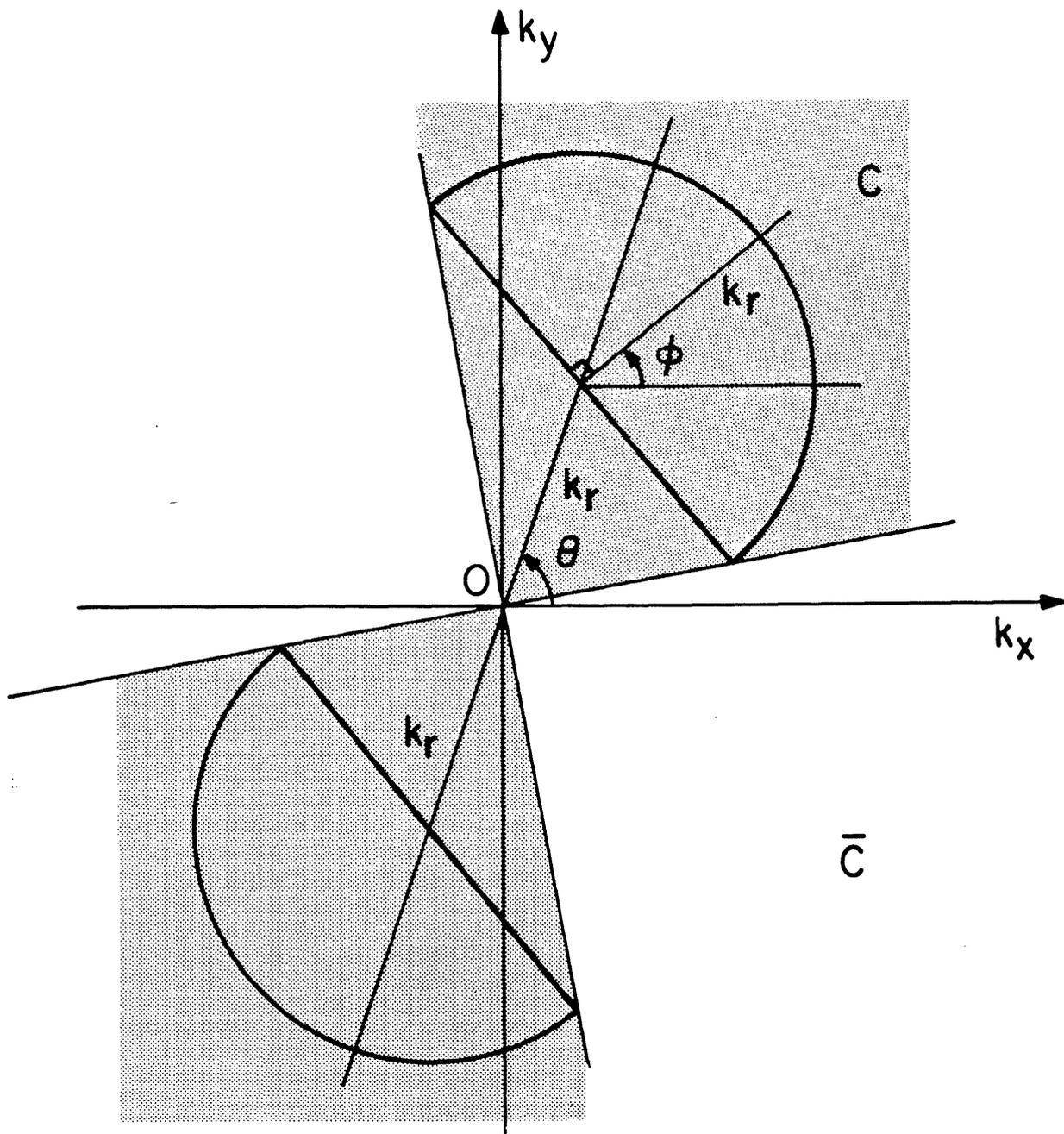
Fig. 3

Fig. 4

Fig. 5

Fig. 6

Fig. 7

Fig. 8

Fig. 9

Fig. 10

Fig. 11